



HAL
open science

Activation of the LicT transcriptional antiterminator involves a domain swing/lock mechanism provoking massive structural changes.

Marc Graille, Zhou Cong-Zhao, Véronique Receveur-Bréchet, Bruno Collinet, Nathalie N. Declerck, Herman van Tilbeurgh

► To cite this version:

Marc Graille, Zhou Cong-Zhao, Véronique Receveur-Bréchet, Bruno Collinet, Nathalie N. Declerck, et al.. Activation of the LicT transcriptional antiterminator involves a domain swing/lock mechanism provoking massive structural changes.. *Journal of Biological Chemistry*, 2005, 280 (15), pp.14780-14789. 10.1074/jbc.M414642200 . hal-02680804

HAL Id: hal-02680804

<https://hal.inrae.fr/hal-02680804>

Submitted on 31 May 2020

HAL is a multi-disciplinary open access archive for the deposit and dissemination of scientific research documents, whether they are published or not. The documents may come from teaching and research institutions in France or abroad, or from public or private research centers.

L'archive ouverte pluridisciplinaire **HAL**, est destinée au dépôt et à la diffusion de documents scientifiques de niveau recherche, publiés ou non, émanant des établissements d'enseignement et de recherche français ou étrangers, des laboratoires publics ou privés.

Activation of the LicT Transcriptional Antiterminator Involves a Domain Swing/Lock Mechanism Provoking Massive Structural Changes*[§]

Received for publication, December 29, 2004, and in revised form, January 28, 2005
Published, JBC Papers in Press, February 7, 2005, DOI 10.1074/jbc.M414642200

Marc Graille^{‡§}, Cong-Zhao Zhou^{¶||}, Véronique Receveur-Bréchet^{**}, Bruno Collinet[¶],
Nathalie Declerck^{‡§§}, and Herman van Tilbeurgh^{‡¶¶}

From the [‡]Laboratoire d'Enzymologie et Biochimie Structurales, CNRS-UPR9063, Bâtiment 34, 1 Avenue de la Terrasse, 91198 Gif sur Yvette, France, the [¶]Institut de Biochimie et de Biophysique Moléculaire et Cellulaire, CNRS-UMR8619, Université Paris-Sud, Bâtiment 430, 91405 Orsay, France, ^{**}Architecture et Fonction des Macromolécules Biologiques, CNRS-UMR6098, Université d'Aix-Marseille I et II, 31 chemin Joseph Aiguier, 13402 Marseille CEDEX 20, France, the ^{‡§}Centre de Biochimie structurale, CNRS-UMR9955/Université de Montpellier I/INSERM U414, 29 rue de Navacelles, 34090 Montpellier, France, and ^{§§}Microbiologie et Génétique Moléculaire, CNRS/INRA/INA-PG UMR2585, 78850 Thiverval Grignon, France

The transcriptional antiterminator protein LicT regulates the expression of *Bacillus subtilis* operons involved in β -glucoside metabolism. It consists of an N-terminal RNA-binding domain (co-antiterminator (CAT)) and two phosphorylatable phosphotransferase system regulation domains (PRD1 and PRD2). In the activated state, each PRD forms a dimeric unit with the phosphorylation sites totally buried at the dimer interface. Here we present the 1.95 Å resolution structure of the inactive LicT PRDs as well as the molecular solution structure of the full-length protein deduced from small angle x-ray scattering. Comparison of native (inactive) and mutant (constitutively active) PRD crystal structures shows massive tertiary and quaternary rearrangements of the entire regulatory domain. In the inactive state, a wide swing movement of PRD2 results in dimer opening and brings the phosphorylation sites to the protein surface. This movement is accompanied by additional structural rearrangements of both the PRD1-PRD1' interface and the CAT-PRD1 linker. Small angle x-ray scattering experiments indicate that the amplitude of the PRD2 swing might even be wider in solution than in the crystals. Our results suggest that PRD2 is highly mobile in the native protein, whereas it is locked upon activation by phosphorylation.

Protein phosphorylation is universally used as a mechanism for signal transduction in all branches of the kingdom of life (1). Despite the simplicity of this chemical modification, the impact

* This work was supported by grants from the Ministère de la Recherche et de la Technologie (Programme Génopoles) and the Association pour la Recherche contre le Cancer (to M. G.). The costs of publication of this article were defrayed in part by the payment of page charges. This article must therefore be hereby marked "advertisement" in accordance with 18 U.S.C. Section 1734 solely to indicate this fact.

[§] The on-line version of this article (available at <http://www.jbc.org>) contains a supplemental figure.

The atomic coordinates and structure factors (code 1TLV) have been deposited in the Protein Data Bank, Research Collaboratory for Structural Bioinformatics, Rutgers University, New Brunswick, NJ (<http://www.rcsb.org/>).

[§] Both authors contributed equally to this work.

^{||} Present address: School of Life Science, University of Science and Technology of China, Hefei Anhui, 230027, China.

^{¶¶} To whom correspondence should be addressed. Tel.: 33-1-69-15-31-55; Fax: 33-1-69-85-37-15; E-mail: Herman.Van-Tilbeurgh@ibbmc.u-psud.fr.

on protein structure and dynamics can be dramatic. Over the last decade, our knowledge of the structure of protein kinases and their targets has increased tremendously. In most cases, however, knowledge of the structure of the phosphorylated state of a protein remains beyond reach. This is mainly due to the difficulty of getting enough fully homogeneously phosphorylated protein for structural studies. Questions on the structural effects of phosphorylation are therefore often addressed using mutants that mimic the phosphorylated state.

The expression of many catabolic operons in bacteria is controlled by (de)phosphorylation of regulatory proteins as exemplified by transcriptional antitermination. LicT from *Bacillus subtilis* belongs to a family of transcriptional antiterminator proteins that control the expression of genes involved in carbohydrate metabolism. LicT modulates the induction of the *licS* gene and the *bglPH* operon involved in the utilization of aryl- β -glucosides and β -glucanases (2, 3). Other well studied members of this family are *B. subtilis* SacY (4) and *Escherichia coli* BglG (5). In the absence of the "inducer" sugar, palindromic mRNA sequences (transcription terminators) located in the leader or intercistronic regions of an operon fold as stem-loop structures, causing detachment of RNA polymerase from the mRNA matrix and leading to truncated transcripts. In the presence of the "inducer" sugar, the antiterminator proteins prevent formation of these RNA terminator stem-loop structures by interacting with an antiterminator RNA sequence (RAT),¹ which partially overlaps with the terminator, hence allowing transcription through the operon (4). Antiterminator proteins from the LicT/BglG family have a modular nature (6). The RNA binding activity resides in the N-terminal domain (termed the co-antiterminator (CAT)) comprising 55 residues. Crystallographic and NMR structural studies of the CAT domain, alone or in complex with its RAT target: showed that it folds as a β -stranded homodimer (7, 8). The NMR solution structure of the CAT:RAT complex elucidated how a symmetric dimer interacts with an apparently asymmetric RNA target (9). In the full-length protein, the ability of CAT to bind RNA and prevent the premature arrest of transcription is controlled by two contiguous regulatory domains termed PRD1 and PRD2. These domains respond to regulation signals sent by the bacterial phosphoenolpyruvate:sugar phosphotransferase system (PTS)

¹ The abbreviations used are: RAT, ribonucleotidic antiterminator; CAT, co-antiterminator; PTS, phosphotransferase system; PRD, PTS regulation domain; SAXS, small angle x-ray scattering.

(10). Each PTS regulation domain (PRDs) comprises about 100 amino acids including two highly conserved histidines. Duplicated PRDs are also found in bacterial transcriptional activators such as LevR and MtlR, which possess not an RNA-binding but a DNA-binding domain at their N terminus (11). In all PRD-containing regulators, the conserved histidines are substrates for reversible phosphorylation by the PTS components, HPr, and/or the sugar specific permeases, Enzymes II. These histidines are (de)phosphorylated in response to the availability of carbon sources, and their phosphorylation state determines the activation state of the transcriptional regulators. In the case of LicT, activation needs dephosphorylation on PRD1 and phosphorylation on PRD2.

We have previously determined the crystal structure of the LicT regulatory domain (LicT-PRD, comprising the CAT-PRD1 linker, PRD1 and PRD2 domains) from a constitutively active double mutant (12). In this activated form, the two conserved histidines of PRD2 (His²⁰⁷ and His²⁶⁹) were replaced by aspartic acids. The charges introduced by these mutations yielded a functionally active mutant that was no longer subject to regulation. Each PRD consists of a five-helix bundle and forms homodimer in the activated protein. Surprisingly in this active dimer, all of the phosphorylation sites are completely buried at the center of the PRD1/PRD1' or PRD2/PRD2' interfaces, hence making them not available for (de)phosphorylating partners (13). Biochemical and biophysical characterization indicated that, although both the native and the activated mutant proteins are dimeric in solution, the mutations induce considerable changes in the tertiary and quaternary structure that lead to dimer rearrangement and stabilization. It was thus proposed that the activation of LicT by phosphorylation of His²⁰⁷ and His²⁶⁹ arises from a conformational switch that stabilizes an active dimeric conformation. The hypothesis was that in the native state, the protein is essentially present as an open dimer where the phosphorylatable histidines are accessible and that upon activation, long range rearrangements would be induced, burying the phosphorylated histidines at the dimer interface and stabilizing a closed conformation efficient for RNA binding. We observed, however, that upon dilution native LicT tends to dissociate into monomers, and therefore the monomeric form may precede the dimer under physiological conditions.

In the present paper we have determined the crystal structure of the native, inactive form of the LicT regulatory domain. The structure shows a dramatically modified configuration of the dimer that opens up and brings the phosphorylatable PRD2 histidines to the protein surface where they become fully accessible to phosphorylating partners. This results from a wide 180° swing movement of the PRD2, which becomes monomeric within the native LicT-PRD. The opened (native) and closed (mutant) LicT-PRD conformations as observed in the respective crystal structures were confirmed by small angle x-ray scattering (SAXS) experiments, suggesting that the PRD2 swing amplitude may be larger in solution than in the crystal. Finally the overall conformation of full-length wild type or mutant LicT was investigated by SAXS experiments. Our results suggest that wild type LicT would be present in solution as a mixture of the active form and of an open form where only PRD1 is involved in dimerization.

MATERIALS AND METHODS

Protein Preparation and Crystallization—The native LicT-PRD protein was essentially purified as described (8). The cell pellets from a 250-ml culture were resuspended in 30 ml of a buffer containing 50 mM phosphate buffer, pH 8, 500 mM NaCl, and 20 mM β -mercaptoethanol. The cells were opened by three rounds of freeze/thaw in liquid nitrogen followed by sonication. The His-tagged proteins were purified on a nickel-nitrilotriacetic acid resin (Qiagen Inc.) column. The protein was

eluted with 300 mM imidazole from the nickel-nitrilotriacetic acid column, and the pooled fractions were loaded on a SuperdexTM 75 (Amersham Biosciences) column equilibrated in 300 mM NaCl, 20 mM Tris, pH 8, 20 mM β -mercaptoethanol. After gel filtration, the protein fractions were pooled and concentrated to 6 mg/ml. The purity of the protein was checked by SDS-PAGE and mass spectrometry. The selenium-methionine-labeled protein was obtained using standard procedures and purified as the native one.

The crystallization of the native LicT-PRD protein was poorly reproducible, and the quality of the crystals was usually mediocre. The native crystals were obtained with the hanging drop vapor diffusion method after 3 months from a 1/1- μ l mixture of protein (at 6 mg/ml in 300 mM NaCl, 20 mM Tris, pH 8, 20 mM β -mercaptoethanol) and crystallization liquid (0.5–0.7 M potassium acetate, 0.1 M sodium citrate, pH 3.4). Selenium-methionine-modified protein crystals were grown in 1 week from a 1/1- μ l mixture of protein (6 mg/ml in 300 mM NaCl, 20 mM Tris, pH 8, 20 mM β -mercaptoethanol) and a reservoir solution of 1.0 M ammonium phosphate, pH 5.0. All of the crystallization trials were performed at 18 °C.

Determination of the Structure—The data on the native crystal were collected on the ID14-EH1 beam line at the European Synchrotron Radiation Facility (Grenoble, France) to a resolution of 1.9 Å. All of the data were reduced using the HKL package (28, 29). Although the native protein has only two different residues from the constitutively activated H207D/H269D double mutant, the structure could not be solved entirely by molecular replacement. A slightly contrasted solution was found with only the PRD1 part of the structure as a search model, using the program CNS (30). This partial structure (about 40% of the total) was not sufficient to phase for the rest of the protein. We therefore prepared a selenium-methionine-labeled LicT-PRD protein sample. The selenium-labeled version of native LicT-PRD was even harder to crystallize than the native protein, and we obtained diffraction data from only one crystal. A partial (80% completed) three-wavelength multiple anomalous diffraction data set at about 2.7 Å could be collected on the French CRG BM30A beam line (European Synchrotron Radiation Facility). Analysis of the anomalous Patterson maps using the SOLVE/RESOLVE program revealed four of six possible selenium positions (31). The selenium sites from the PRD1 were compatible with methionine positions resulting from the molecular replacement solution for this domain. The resulting maps were not of sufficient quality to construct the whole LicT-PRD, but the presence of some helical regions confirmed the molecular replacement solution found for PRD1. Clear electron density was also observed for two helices of PRD2. Multiple anomalous diffraction and MR phases were combined using the CCP4 suite of programs (32). The combined maps allowed completion of the PRD2 structure. This model was then further refined against the native data. Final refinement statistics are summarized in Table I. Only very poor density was present for the region between residues 221 and 236, and these are not present in the final model. The atomic coordinates and structure factors for the native LicT-PRD structure have been deposited into the Brookhaven Protein Data Bank under the accession number 1TLV.

Small Angle X-ray Scattering—Small angle x-ray scattering experiments were performed on the D24 instrument installed on the bending magnet of the storage ring Laboratoire pour l'utilisation du Rayonnement Electromagnétique (Orsay, France). The wavelength was 1.488 Å, and the sample-to-detector distance was 1.40 m. The vertical linear-sensitive position detector was shifted upwards with respect to the incident beam so that the scattered intensity for higher scattering angles could be measured. This set-up gave access to scattering vectors q ranging from 0.015 to 0.27 Å⁻¹. The scattering vector is defined as $q = 4\pi/\lambda \sin\theta$, where 2θ is the scattering angle. Eight to sixteen frames of 200 s were recorded depending on the protein concentration. The protein solution was continuously circulated through the evacuated quartz capillary so that no radiation-induced damage was observable, and individual frames could then be averaged. Absolute calibration was made with samples of lysozyme and bovine serum albumin of known concentrations. A series of measurements at different protein concentrations ranging from 1 to 11 mg/ml were performed for each protein to check for interparticle interaction. Background scattering (buffer was 50 mM Na₂HPO₄, pH 7.0, 100 mM Na₂SO₄, 2 mM dithiothreitol, 1% (v/v) glycerol) was measured before or after each protein sample using the corresponding buffer solution and then subtracted from the protein scattering patterns after proper normalization and correction from detector response. All of the experiments were conducted at 20 °C.

The theoretical scattering functions based on the atomic coordinates of the crystal structures or of models were calculated using CRY SOL (16). They were fitted to the experimental data by taking into account

TABLE I
Data collection and refinement statistics

	Native data	Selenium edge	Selenium peak	Selenium remote
Wavelength (Å)	0.934	0.9803	0.9800	0.9825
Unit cell parameters (Å)	$a = b = 48.73, c = 162.47$	$a = b = 48.8, c = 166.2$		
Resolution (Å)	99–1.90	25–2.66	25–2.74	25–2.73
Number of reflections	159,143	22,532	19,937	20,391
Number of unique reflections	18537	6633	6003	6519
R_{merge} (highest resolution shell) ^a	0.036 (0.40)	0.054 (0.38)	0.055 (0.41)	0.039 (0.55)
$I/\sigma(I)$ (highest resolution shell)	44.7 (5.5)	14.2 (2.2)	14.2 (2.0)	14.2 (1.7)
Overall completeness (%)	99.4	91.3	90.3	90.3
Refinement				
Resolution (Å)	10–1.95			
Reflections (working/test)	16547/821			
$R_{\text{cryst}}/R_{\text{free}}^b$	0.269/0.292			
Residues	205			
Nonhydrogen atoms	1697			
Water molecules	98			
Root mean square deviation				
Bonds (Å)	0.007			
Angles (°)	1			
Ramachandran analysis (%)				
Most favored	97			
Allowed	3			

^a $R_{\text{sym}} = \sum_i \sum_h |I_{hi} - \langle I_h \rangle| / \sum_h \sum_i I_{hi}$, where I_{hi} is the i th observation of the reflection h , while $\langle I_h \rangle$ is the mean intensity of reflection h .

^b $R_{\text{factor}} = \sum ||F_o| - |F_c|| / \sum |F_o|$. R_{free} was calculated with a small fraction (4.8%) of randomly selected reflections.

the excluded volume and the scattering by a hydration shell having a slightly different density than the bulk solvent.

RESULTS

Native and Mutant LicT-PRDs Have Radically Different Structures—Several lines of evidence raised by experiments conducted in solution converged toward the hypothesis that the conformations of wild type inactive LicT and of the constitutive active LicT-H207D/H269D double mutant (or of the corresponding LicT-PRDs) are radically different (8, 13). One single crystal of native LicT-PRD allowed good quality x-ray diffraction data to a resolution of 1.9 Å to be recorded (Table I). Molecular replacement using separately the structures of PRD1 and PRD2 of the double mutant as search models only gave a solution for PRD1 (comprising residues 67–166). The complete structure of LicT-PRD was finally solved by including multiple wavelength anomalous dispersion data obtained from a selenomethionine-substituted (selenium-methionine) crystal (14). In the final model refined to 1.95 Å resolution, the electron density of LicT-PRD is well defined except for the region comprising residues 222–235, which corresponds to the PRD2 $\alpha 3$ helix in the mutant. Mass spectrometry analysis proved that the crystals contain intact protein, and therefore the poor density of this region must be due to conformational mobility. In the mutant, the $\alpha 3$ helix is involved in dimer packing, but, as discussed further, this interface is absent in the native structure. This region seems prone to mobility, because neither residue Glu²²² nor Ser²²³ was visible in the mutant structure.

Structural Comparison of Native and Mutant LicT-PRD Monomer—LicT-PRD is made up of duplicated five-helix bundle domains (PRD1 and PRD2) connected by a short linker. In the mutant, few interactions exist between the two modules, and the monomer has an elongated shape (longest C α distance of about 60 Å). In the native form, PRD2 closes in upon PRD1, resulting in a more compact monomer (longest C α of about 51 Å). As represented in Fig. 1a, the overall structure of the two modules is maintained in the present native LicT-PRD (see further), but their relative orientation and position are very different compared with the mutant. The superposition of native and mutant LicT-PRD monomer structures on PRD1 very clearly illustrates the swing movement of PRD2. This drastic reorientation of PRD2 relative to PRD1 is entirely because of a change in main chain conformation of a few residues in the short connection contained between residues 165 and 170 (Fig.

1a, bottom inset). Two main switches are clearly identified: one at residues Leu¹⁶⁵ and Asn¹⁶⁶ whose Ramachandran (Φ , Ψ) angles change, respectively, from -61° , -15° and -81° , 3° in the mutant to -94° , -179° and 57° , 51° in the native LicT-PRD and the other at residue Met¹⁶⁹ whose (Φ , Ψ) angles change from -120° , 93° in the mutant to -40° , -54° in the native structure. Through these backbone conformational changes, PRD2 rotates by 180° compared with its position in the mutant, bringing PRD2 in closer contact to PRD1 of the same monomer (Fig. 1b). This rearrangement considerably increases PRD1-PRD2 interactions through packing of hydrophobic patches on the protein surface (Leu¹¹⁸, Leu¹²⁵, and Leu¹⁵⁸ on PRD1 and Met¹⁶⁹, Ile¹⁷², Ile¹⁷³, Leu¹⁸³, and Val²⁰⁵ on PRD2) and formation of new hydrogen bonds, involving Arg¹²⁴/Tyr²⁰¹, Tyr¹²⁶/Thr¹⁷⁶, and Glu¹⁶⁷/Gln²¹³.

Remodeling of the Dimer—Measurements in solution (gel filtration, ultracentrifugation, and SAX) indicated that both the native and mutant LicT-PRD are dimeric but that the native dimer is less stable and less compact (8). As for the mutant crystals, the native LicT-PRD dimer is generated by a crystallographic 2-fold axis. A comparison of the native and mutant LicT-PRD dimer structures is represented in Fig. 2. The mutant LicT-PRD forms an extensive dimer burying 3400 Å² and characterized by roughly equal PRD1/PRD1' and PRD2/PRD2' interaction surfaces and very few PRD1/PRD2' interactions (prime refers to the other monomer; Fig. 2b). PRD1 and PRD2 each form a quasi-independent dimeric unit with the $\alpha 2$ and $\alpha 5$ helices (containing the phosphorylation sites) from one monomer facing the corresponding helices in the other monomer. Although the PRD1/PRD1' association is rather loose, the PRD2/PRD2' contacts involve tight electrostatic and hydrophobic interactions (see below).

Although the interface of the native dimer shrunk to a value of 1707 Å² (Fig. 2a; 50% of the buried surface of the mutant dimer), it remains within the range observed for dimers (15). The PRD2 swing totally removes this module from the native interface, causing a complete remodeling of the corresponding native dimer, and reduces PRD2/PRD2' interactions to packing of a small hydrophobic patch at the N terminus of the $\alpha 1$ helices. The PRD1/PRD1' dimer interface has partially opened up and is only loosely stabilized by hydrophobic packing of the $\alpha 2$ helices. The short PRD1-PRD2 connecting segment (residues 165–170), whose change in orientation is responsible for

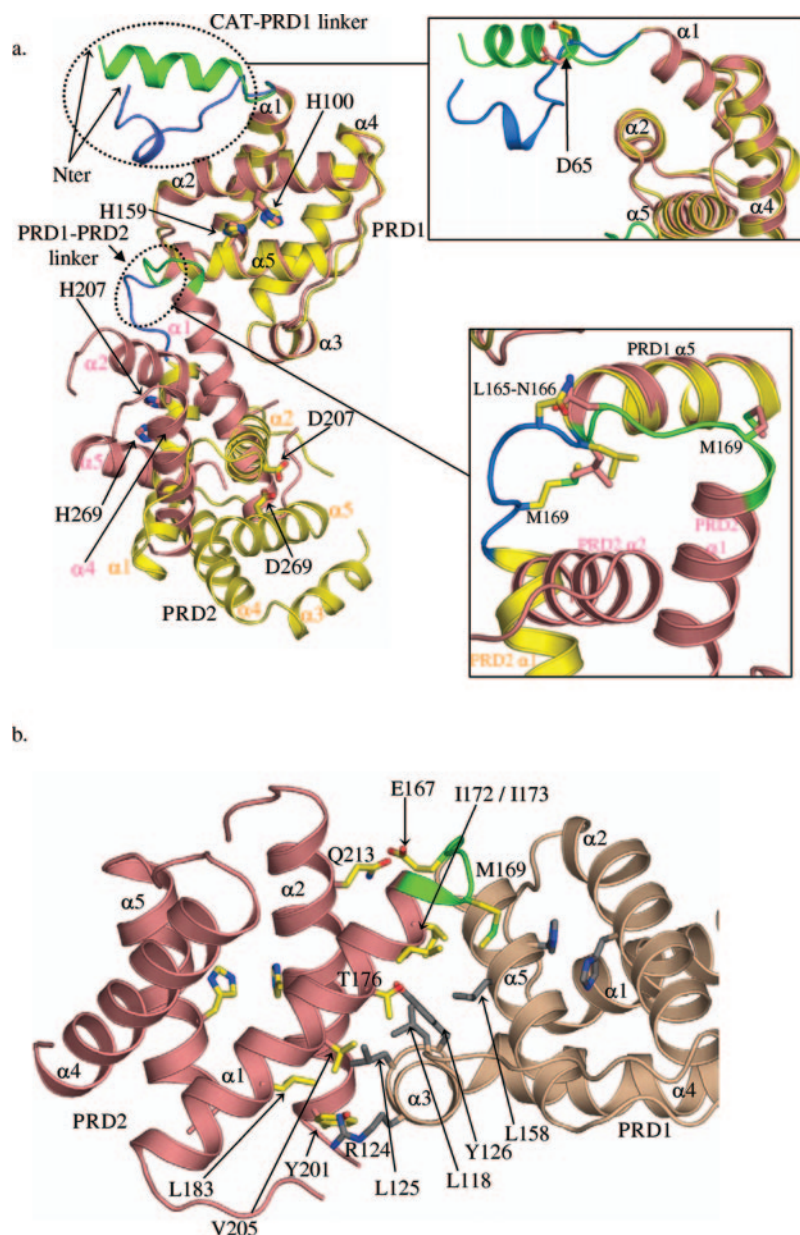


FIG. 1. Structural changes of LicT-PRD. *a*, structural comparison of native (pink) and mutant (yellow) LicT-PRD monomers, superimposed onto PRD1. The CAT-PRD1 linker and the PRD1-PRD2 hinge region of the native and mutant proteins are colored green and blue, respectively. Structural elements for the PRD2 domain of the mutant LicT monomer are labeled in the corresponding colors. *Top inset*, zoom on the CAT-PRD1 linker. *Bottom inset*, zoom on the hinge region connecting PRD1 to PRD2. For clarity, amino acid single-letter codes are used. *b*, PRD1-PRD2 interface in the native protein. PRD1, PRD2, and the linker connecting both domains are colored light brown, pink, and green, respectively.

the LicT-PRD swing, becomes inserted between the PRD1 $\alpha 5$ helices and forms two intermolecular salt bridges with the PRD1 $\alpha 2$ helices (Glu¹⁶⁷/Arg¹⁰⁷ and Glu¹⁶⁸/His¹⁰⁰). To accommodate the PRD1-PRD2 connecting segment at the PRD1/PRD1' interface, one PRD1 has pivoted relative to the other and slid toward the CAT-PRD1 linker (Fig. 3*a*). During this sliding movement, the C terminus of the $\alpha 1$ helix has moved by 13 Å, and the N-terminal of the CAT-PRD1 linker has moved by 7 Å. This repositioning of the PRD1 monomers also induced side chain movements in the immediate vicinity of the phosphorylation sites (see below).

PRD1/PRD2' interactions involve the PRD1 segment comprising residues 112–125. In the mutant this segment contacts the N termini of helices $\alpha 1$ and $\alpha 2$ in PRD2', whereas in the native form, it contacts the turns at the N termini of helices $\alpha 2$ and $\alpha 4$. Upon this rearrangement, one PRD1/PRD2' electrostatic interaction is lost (between Glu¹²¹ and Lys²⁰⁹) and one is created (between Asn²¹⁶ and Asp¹¹³).

Secondary Structure Formation at the CAT-PRD1 Linker—PRD1 is connected to the RNA-binding domain through a linker region comprising residues 56–67. The electron density map of this region is well defined in both the wild type and

mutant crystal structures. In the mutant, the linker contains one helical turn (residues 57–59), whereas the remaining residues adopt an extended conformation. The entire native linker (residues 56–65), however, forms an amphipathic helix. In the dimer, both linkers form an anti-parallel helical bundle through packing of their hydrophobic surfaces (Phe⁵⁹, Leu⁶², Leu⁶³, and Ile⁶⁶), thereby considerably stabilizing the dimer interface. The linker in fact provides 30% of the total native dimer interface. In native LicT-PRD, the two linker helices lie on top of the PRD1/PRD1' interface, against a small hydrophobic patch comprising Met⁷¹, Tyr⁹¹, and Val⁹⁵ from helices $\alpha 1$ and $\alpha 2$ of both monomers. The same hydrophobic patch is contacted by the extended linker region in the mutant, but side chain interactions are totally different. Two of the hydrophobic residues forming the amphipathic helix of the native linker (Phe⁵⁹ and Leu⁶³) are partially exposed to the solvent in the mutant, whereas Tyr⁶⁴, which is exposed to the solvent in the native form, is buried and makes a hydrogen bond interaction with Asp⁹⁹ in the mutant form.

As illustrated in the *top inset* of Fig. 1*a*, the linker radically changes direction at residue Asp⁶⁵ between native and mutant LicT-PRD, repositioning it relative to PRD1. Therefore the

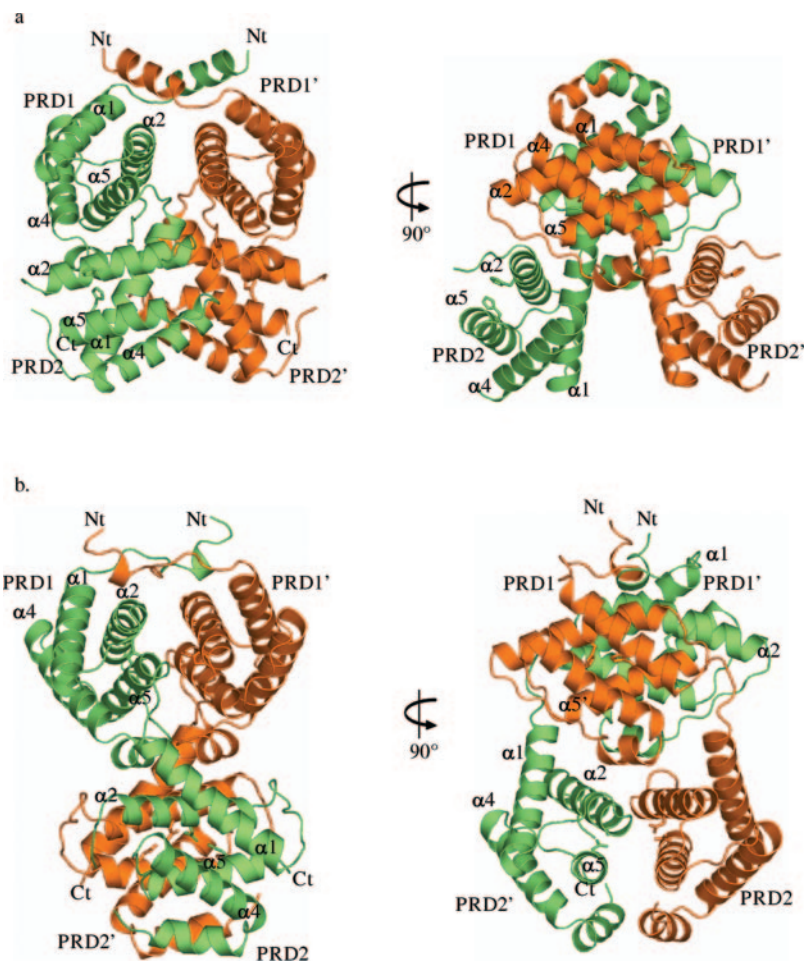


FIG. 2. Comparison of native and mutant LicT-PRD dimers. Ribbon presentations of the native (a) and mutant (b) LicT-PRD dimer. The two monomers are in green and orange, respectively. The left and right panels are related by a 90° rotation around the vertical axis. The phosphorylatable residues or the corresponding aspartate mutations are shown as sticks.

N-terminal residue of the linker (Glu⁵⁷), corresponding to the C-terminal residue of CAT has moved over a distance of 7 Å (Fig. 3a). Undoubtedly, if the same linker configurations of native and mutant LicT-PRD are present in the corresponding intact versions of LicT, this movement will certainly affect the CAT dimer (see below).

Structural Changes within PRD1 and PRD2—To gain deeper insight into the structural effects of the activating mutations, we have compared native and mutant PRD1 and PRD2 individually (Fig. 3). The backbone of the five-helix bundle forming PRD1 is almost identical between the native and mutant (RMSD value of 0.6 Å for 101 C α positions; Fig. 3b). Relevant structural changes are limited to 1) different side chain conformations occurring at residues Asp⁹⁹, Phe¹⁰³, Arg¹⁰⁷, Trp¹²⁰, and Arg¹²⁴ and 2) the $\alpha 2/\alpha 3$ loop region comprising residues 109–114. All of these residues are involved in intermolecular contacts that are not maintained between the native and mutant dimers.

Although the overall structure of native and mutant PRD2 is very similar, the relative positions of its helices change considerably. The best superposition of PRD2 yields a RMSD of 1.7 Å for 95 C α positions, mainly contributed by a rigid movement of the $\alpha 1/\alpha 2$ helices (carrying His²⁰⁷) relative to the $\alpha 4/\alpha 5$ helices (carrying His²⁶⁹). The corkscrew movement of the $\alpha 1$ helix is a combination of a rotation around the helical axis and a translation of about 2.5 Å along the helical axis (Fig. 3c). The movement of the $\alpha 2$ helix is a combination of a 4 Å translation with a 15° tilt of the helical axis, loosening the packing of the $\alpha 2$ and $\alpha 5$ helices in native compared with mutant PRD2. Relevant side chain reorientations occur at positions Arg²⁰³, Phe²¹⁰, Phe²¹¹, Arg²¹⁴, Asp²⁶¹, Tyr²⁶⁵, and Arg²⁷², all located at the

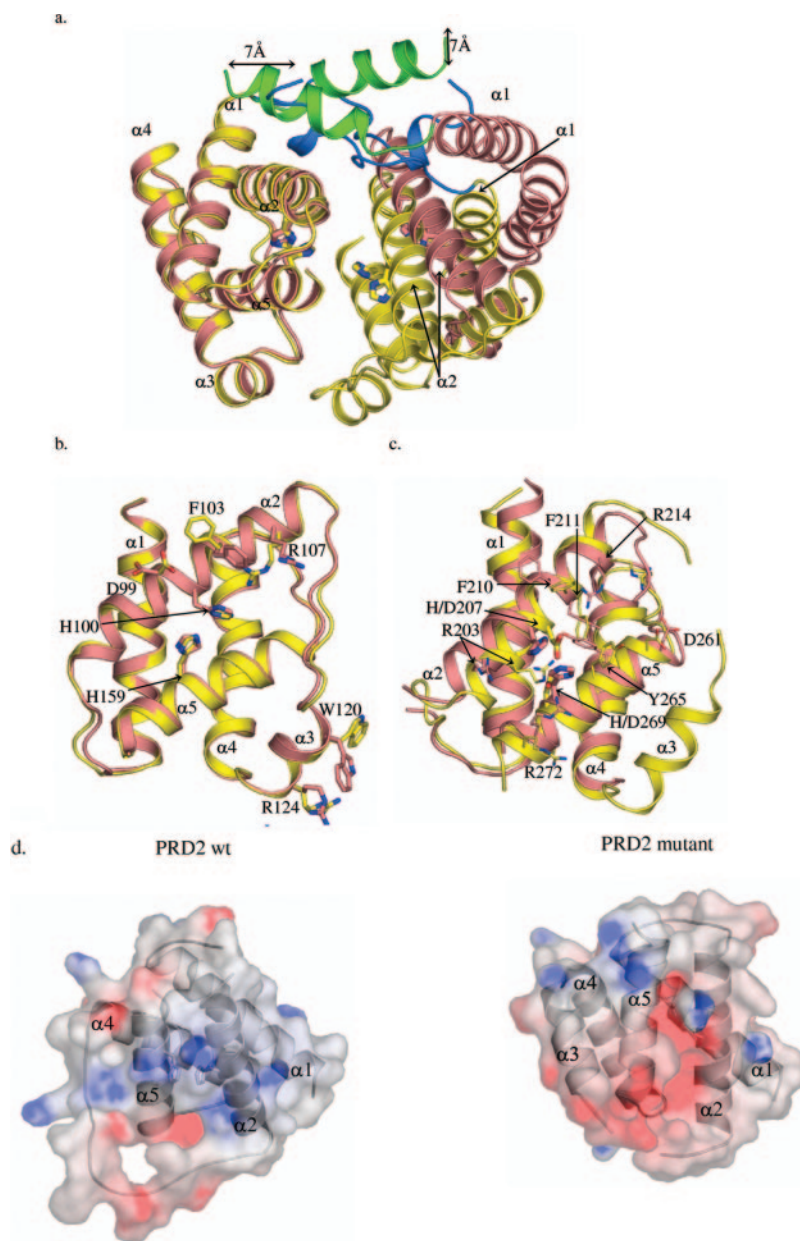
PRD2/PRD2' interface in the mutant but exposed to solvent in the native form, except Phe²¹¹, whose side chain is buried between $\alpha 2$ and $\alpha 5$.

The PRD1 and PRD2 Phosphorylation Sites—The helices $\alpha 2$ and $\alpha 5$ of PRD1 and PRD2 each carry conserved histidines that are phosphorylation targets for PTS proteins (His¹⁰⁰/His²⁰⁷ and His¹⁵⁹/His²⁶⁹). Folding brings the phosphorylation sites in close contact within each module. In mutant PRD2, Asp²⁰⁷ and Asp²⁶⁹, corresponding to the phosphorylation sites are buried at the dimer interface and contribute to dimer formation and stabilization. Together with Arg²⁰³, Asp²⁰⁷, and Asp²⁶⁹ form a tight intermolecular interaction network. In their immediate vicinity lie conserved aromatic residues (Phe²¹⁰ and Tyr²⁶⁵), and on the edge, there is a large hydrophobic patch comprising Leu²⁶⁴ and Ile²⁶⁸ from the $\alpha 5$ helix and Phe²²⁷, Leu²²⁸, Val²³², and Tyr²³⁵ from helix $\alpha 3$, whose side chains also contribute to dimer stabilization (Fig. 3c). Because of the 180° swing of native PRD2, His²⁰⁷ and His²⁶⁹ are removed from the dimer interface and become freely accessible to phosphorylating partners. They are still in close contact to each other, but a change in side chain orientation compared with those from Asp²⁰⁷ and Asp²⁶⁹ in the mutant creates a tight intramolecular interaction network with Tyr²⁶⁵. Three arginine side chains, which were forming intra or intermolecular salt bridges (Arg²⁰³/Asp²⁰⁷, Arg²¹⁴/Glu²⁶², and Arg²⁷²/Asp²²⁵/Asp²⁶¹) in the mutant structure, were then unpaired and create a positively charged environment around the phosphorylation sites (Fig. 3, c and d).

Despite the fact that the native PRD1/PRD1' interface has opened and hence phosphorylatable histidines have become solvent-accessible, the PRD1 His¹⁰⁰/His¹⁵⁹ remain sterically beyond reach to phosphorylating partner proteins. Phosphoryl-

FIG. 3. Phosphorylatable residues at the dimer interfaces.

a, superimposition of the native (*pink*) and mutant (*yellow*) PRD1 part of the dimer. The figure was generated by superposing only one PRD1 subunit. The native and mutant CAT-PRD1 linkers are represented in *green* and *blue*. The 7Å movement of the N-terminal linker residues is indicated. *b* and *c*, superimposition of the individual mutant (*yellow*) PRD1 (*b*) or PRD2 (*c*) domains onto the corresponding native ones (*pink*). Residues adopting different conformations in the mutant and native domains are shown as *sticks*. *d*, representation of the electrostatic potential surface of the PRD2 domain in the LicT-PRD native (*left*) and mutant (*right*) structures, facing the phosphorylation sites. The positively and negatively charged surface potentials are colored *blue* and *red*, respectively.



ation of His¹⁰⁰/His¹⁵⁹ clearly requires either a still very different dimer arrangement or dissociation into monomers. Although the structure of PRD1 changes very little between native and mutant LicT-PRD, the environments of its phosphorylatable histidines are slightly different. The side chains of His¹⁰⁰ and His¹⁵⁹ remain in the same position and orientation, but their interactions with surrounding residues are different in both structures (Fig. 3*b*).

LicT in Solution as Seen by SAXS—Previous SAXS experiments and extracted molecular parameters have been published previously (8). It was shown that native and mutant versions of intact LicT and LicT-PRD all exist as dimers in solution and that the mutant constructs have a significantly reduced radius of gyration (R_g) compared with the native forms (8). For instance the R_g value for wild type LicT-PRD is 29.5 Å compared with 26.9 Å for LicT-PRD-H207D/H269D. Here, we compare experimental scattering curves obtained in solution with the theoretical scattering curve calculated from the atomic coordinates of the proteins determined by either crystallography or modeling, using the CRY SOL software (16).

The experimental scattering data for mutant LicT-PRD cor-

respond well with the calculated scattering curve using the corresponding crystal structure ($\chi^2 = 3.7$; Fig. 4*a*), indicating that the solution and crystal structures are very similar. On the other hand, the native LicT-PRD crystal structure does not fit as well with native SAXS data (high $\chi^2 = 8.0$ and systematic deviation to the experimental data in the $0.10 \text{ \AA}^{-1} < q < 0.15 \text{ \AA}^{-1}$ region). Similarly, when fitting the closed crystal structure to the native solution data ($\chi^2 = 7.8$), a strong standard deviation persists between medium and large scattering angles ($0.10 \text{ \AA}^{-1} < q < 0.22 \text{ \AA}^{-1}$) (Fig. 4*b*). This indicates that native LicT-PRD adopts in solution a conformation that is different from those in the native or mutant crystals. We have therefore searched for dimer models that would better match the SAXS solution data, starting from the native LicT-PRD crystal structure. Wider opening of the PRD2 modules, obtained through main chain rotations at residues Leu¹⁶⁵ and Met¹⁶⁹ of the native LicT-PRD, resulted in a dimer model that fits much better to the experimental data (χ^2 of 2.3 for the best model (Fig. 4*b*)). These results suggest that in native LicT-PRD, the PRD2 may swing out further in solution than in the crystal.

Because attempts to obtain diffracting crystals of full-length

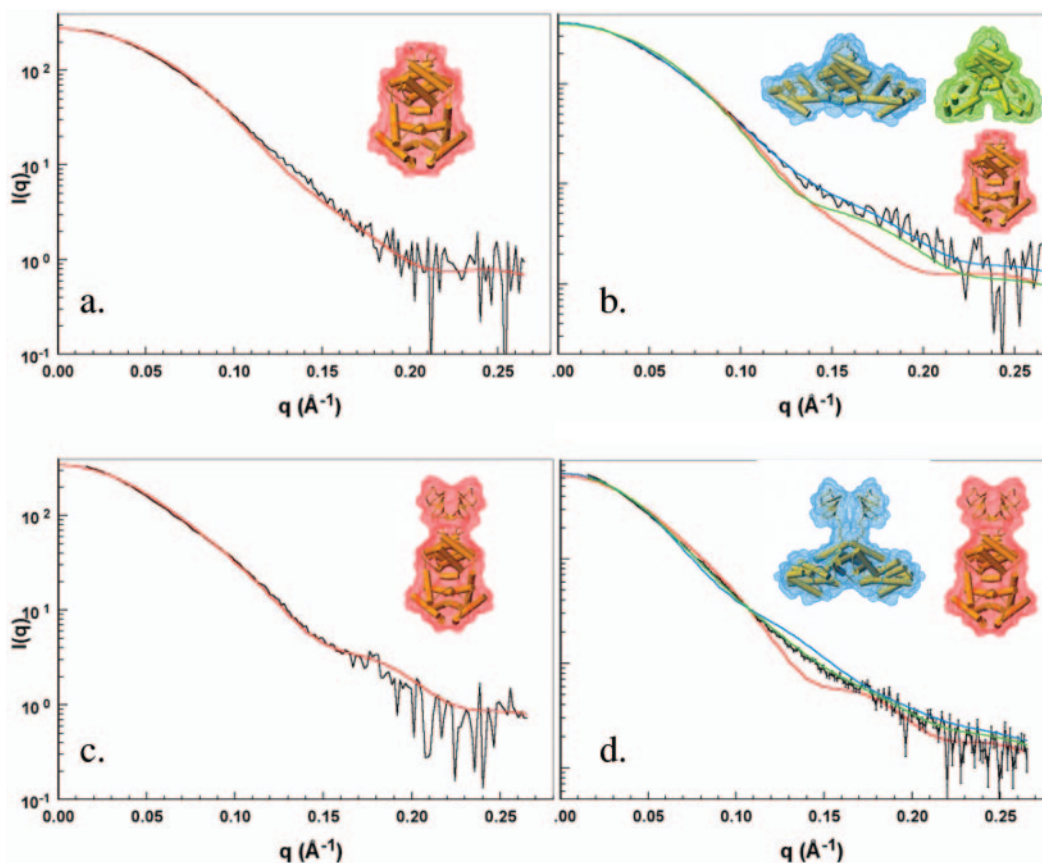


FIG. 4. Experimental and calculated small angle x-ray scattering curves for native and mutant forms of intact LicT and LicT-PRD. *a*, experimental scattering curve (black circles) of mutant LicT-PRD and the calculated fit (red) obtained with CRYSOLO from the corresponding crystal structure ($\chi^2 = 3.7$). *b*, experimental scattering (black circles) curve of native LicT-PRD and fits obtained with CRYSOLO from the crystal structure of native LicT-PRD (green; $\chi^2 = 8.0$), the crystal structure of LicT-PRD mutant (red; $\chi^2 = 7.8$), or a model of LicT-PRD with the PRD2 in the most open conformation (blue; $\chi^2 = 2.3$). *c*, experimental scattering curve (black circles) of mutant intact LicT and fit (red) obtained with CRYSOLO from a model combining individual crystal structures of mutant LicT-PRD and the CAT domain (red; $\chi^2 = 4.1$). *d*, experimental scattering curve (black circles) of full-length native LicT and fit obtained with CRYSOLO from the native model of LicT (red; $\chi^2 = 9.5$), the native model of LicT with PRD2 in the most open conformation (blue; $\chi^2 = 6.6$), or a mixture of these two conformations, whose composition was obtained by OLIGOMER (green; $\chi^2 = 5.7$).

native or mutant LicT failed so far, we undertook further SAXS solution experiments to gain information on the configuration of the CAT domain within the context of intact LicT. A model of mutant full-length LicT, built by end-joining the PRD N terminus and the CAT domain C terminus, yielded a theoretical scattering curve in good agreement with corresponding SAXS measurements (χ^2 of 4.1; Fig. 4c). A similar approach for the native LicT in which we used a model combining the individual dimeric CAT and native LicT-PRD structures resulted in a poor match between calculated and experimental scattering data ($\chi^2 = 9.5$). We then generated a series of models with varying domain openings for CAT and PRD2 domains. The best model ($\chi^2 = 6.6$) was obtained with a slightly more open configuration for both CAT and PRD2 compared with their respective crystal structures. However, the apparent flexibility of LicT suggests that in solution it may be present as a mixture of different conformations. We investigated this possibility by analyzing our SAXS data using the program OLIGOMER (17) that fits the experimental scattering curve of a multi-component mixture of proteins by providing the volume fraction of each component. We have provided OLIGOMER with the scattering form factors as calculated by CRYSOLO from all available models. As illustrated in Fig. 4d, the best result was always obtained by a mixture of 61% of a model with slightly open CAT and wide open PRD2 domains, and 39% of the model of the closed intact and active LicT ($\chi^2 = 5.7$). This suggests that in solution native full-length LicT oscillates between two different

dimer conformations: one very open and the other closed as observed for the active mutant. The D_{\max} values obtained from the experimental scattering curves are much larger than those extracted from our models, showing that much more open models exist in solution. The high number of conformational degrees of freedom (six adjustable modules and probably monomer dimer equilibria) preclude more accurate fitting of our data for intact LicT.

DISCUSSION

Structural (NMR and crystallography) and genetic studies have clearly established that the conditional transcriptional antiterminators from the BglG/SacY family have a common modular organization (4, 6), consisting of multiple well identified structural and functional domains. However, how these different modules communicate and how their phosphorylation regulates antitermination remain open questions. Mutation to aspartate of the two highly conserved histidines of the PRD2 LicT antiterminator (LicT-H207D/H269D) mimics the phosphorylation of the active site histidines of PRD2 responsible for LicT activation. *In vivo* and *in vitro* studies all converged to the conclusion that LicT-H207D/H269D behaved as a permanently phosphorylated antiterminator and that the mutant LicT-PRD adopted the active conformation. Until now, only the structure of an activated mutant form of the LicT regulatory domain was known. By providing a view of an inactive conformation, the present structure of the native LicT-PRD brings us a signifi-

cant step further in the understanding of transcriptional anti-termination at the molecular level.

LicT Is Capable of Adopting Multiple Conformations—In mutant LicT-PRD, phosphorylatable histidines of both PRD1 and PRD2 were all deeply buried at the dimer interface (12). Because these sites should be accessible to phosphorylating protein partners in native LicT, this suggested that LicT must adopt radically different conformations in the native (inactive) and mutant (active) state.

The drastic rearrangement between native and mutant dimer is the response of LicT to the activating mutations forming the basis of the phosphorylation-based mechanism of LicT activation. Biochemical and SAXS analysis of native and mutant LicT (PRD or intact protein) showing that the H207D/H269D activating mutation leads to a more stable and compact dimer are now underpinned by the present crystal structure. Whereas in mutant LicT PRD1-PRD1' and PRD2-PRD2' interfaces equally contribute to the dimer, PRD2-PRD2' interactions are almost totally absent in the native dimer. The PRD2 swings out from the dimer interface to pack against the PRD1 of the same monomer, and most importantly, the PRD2 phosphorylatable histidines on helices $\alpha 2$ and $\alpha 5$ become accessible to the phosphorylating enzyme HPr. The PRD1-PRD1' interactions, although maintained in the native dimer, are considerably diminished and weakened. Dimeric interactions are also completely changed in the region of the CAT-PRD1 linker.

Strikingly, these massive structural rearrangements of the LicT-PRD dimer result from only two main chain conformational switches: at the C-terminal end of the CAT-PRD1 linker (residue 65) and in the short PRD1-PRD2 linker (residues 165 and 169). The state of both switches has crucial structural and functional effects; the latter switch induces the PRD2 swing that converts the phosphorylatable open dimer into a stable closed dimer, whereas the former induces the remodeling of the CAT-PRD1 linker and therefore probably affects the structure and RNA binding activity of the CAT domain in the context of the intact protein.

The ability of native LicT-PRD to adopt alternative conformations is clearly supported by our present small angle x-ray scattering experiments. According to the SAXS curves, native LicT-PRD adopts a more open conformation in solution than in the crystal. This may be partly explained by differences in experimental conditions, in particular buffer pH (acidic for crystallization and neutral for SAXS studies). Main chain rotations at residues 165/169 are sufficient to obtain modeled structures that better fit the experimental native scattering data than the native crystal structure. In these models, the PRD2 swings further out, increasing its packing against PRD1. For the full-length protein, the SAXS data are best explained by the presence of a mixture of an open dimer where the PRD2 swing is maximal and a closed dimer similar to the active form. Native LicT dimers are unstable and tend to dissociate at low protein concentrations, suggesting that there may exist a dynamic equilibrium between monomeric and dimeric forms as well.

Recent genetic and biochemical results on BglG, the LicT ortholog in *E. coli*, provided evidence for the presence of transient conformers in which PRD1 and PRD2 come in close proximity, allowing the transfer of phosphoryl groups (18) or cross-linking of residues (19) between the two modules. These results are not compatible with the structures of the PRDs determined so far and can be explained only by an alternative packing of the PRD1 and PRD2 modules, different from that observed in the crystals of native or mutant LicT-PRD.

The Mechanism of LicT Activation—The above discussed results suggest that the native LicT dimer oscillates between

several conformations, whereas activated LicT, induced either by PRD2 phosphorylation or by mutation(s), is locked in a single closed dimer conformation. Our studies have indeed clearly established that the LicT dimer is stabilized upon activation (8). To our view, understanding the structural mechanism underlying LicT activation boils down to the question: how can PRD2 phosphorylation (or mutation) convert an unstable open dimer into a firmly closed active dimer? Comparison of the native and activated mutant PRD crystal structures shows that PRD2 undergoes a complete reconfiguration of the interaction network within the helix bundle, probably provoked by the change in electrostatic potential and solvent accessibility of its active site surface induced by the His-to-Asp mutations. In the active configuration, the PRD2 helices pack tighter, and salt bridges are established across the PRD2-PRD2' interface, thereby keeping the dimer firmly closed. The PRD2 swing leading to activation also removes the short PRD1-PRD2 connecting segment (residues 165–169) from the PRD1-PRD1' interface. Therefore, the PRD1 monomers can move closer and form a more compact dimer. Disruption of the PRD1-PRD2 interface also brings the PRD1 modules into a more intimate dimer contact. Both modules thus seem to act synergistically to stabilize the closed dimer. As shown in Fig. 3 (*c* and *d*), the His-to-Asp mutations at the PRD2 active sites induce important changes in structure and electrostatic properties of the PRD2-PRD2' interface in the mutant LicT-PRD, promoting its stabilization.

CAT/RAT interaction prevents the formation of an overlapping terminator in the mRNA leader region of the *bglPH* operon and thereby stimulates transcription of this operon (4). This process requires HPr-dependent phosphorylation of PRD2 (8, 20). In LicT, the H207D/H269D mutations mimicking phosphorylation of the PRD2 histidines indeed increase CAT affinity for RAT (8, 12, 20). How do the conformational changes taking place in the regulatory domain regulate CAT RNA binding? Because CAT alone is constitutively active *in vivo*, it is able to bind efficiently to its RAT sequence on its own (6, 21). The NMR structure of the CAT·RAT complex clearly proves that dimer formation is absolutely requested for RAT recognition; RAT binds at the rim of the CAT module and involves residues from both monomers. Disruption or modification of the CAT dimer will necessarily abolish or reduce the affinity for RNA. PRD dimer closure definitely affects the conformation of the CAT-PRD1 linker. The sliding movement at the PRD1-PRD1' interface provokes an almost complete unfolding of the CAT-PRD1 linker helix and a 7 Å movement of the N terminus. Undoubtedly, the linker configurations will affect the structure of the CAT dimer and its ability to bind RNA (see below). We therefore propose that the control of CAT activity relies on a simple oligomerization switch dictated by the overall conformation of the LicT dimer. In native LicT-PRD the helical conformation of the CAT-PRD1 linker, tightly fixed in dimer formation, holds the N terminus in a position that impedes the formation of an active CAT dimer. Modeling of intact mutant LicT shows that because of the extended CAT-PRD1 linker, the positions of the N termini of the PRD are compatible with the active CAT dimer. This conformational switch model is supported by our SAXS experiments on full-length LicT; scattering data on the native protein are best explained by a model in which the CAT dimer is disrupted, whereas for the activated mutant they fit very well to a model where CAT is dimeric and joined to PRD1 through an extended linker (Fig. 4, *c* and *d*).

The mechanism of LicT inactivation involving the conserved histidines of PRD1 (His¹⁰⁰ and His¹⁵⁹) is less well established (20, 22, 23). According to genetic and biochemical studies on LicT and other antiterminators of the BglG/SacY family (20,

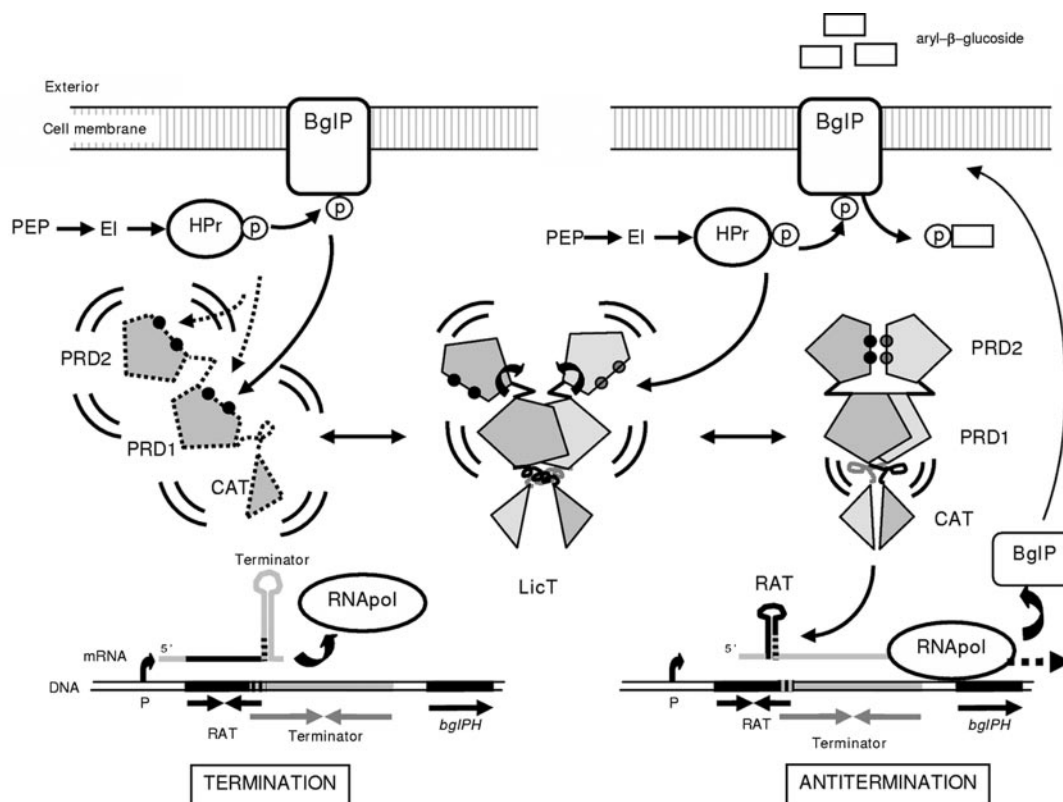


FIG. 5. Proposed model for the phosphorylation-based regulation of LicT antitermination activity. LicT, a multiconformational modular protein, is reversibly phosphorylated at two conserved histidines in PRD2 (black dots) by the PTS system in response to the availability of carbon sources. In the native, unphosphorylated state, LicT is in equilibrium between the (partially folded?) monomer, a more or less open dimer where only PRD1 is dimeric, and a closed active dimer where all the LicT modules are dimeric and the phosphorylation sites are buried at the interface. In the native open dimer (center of the figure), the CAT-PRD1 linker is helical and prevents CAT dimerization, whereas the PRD1-PRD2 linker is highly mobile and allows large PRD2 movements. In this form LicT is unable to bind RNA (bottom left corner) and to prevent the premature termination of transcription of the *bglPH* operon. Phosphorylations of PRD1 catalyzed by BglP at His¹⁰⁰ (and by HPr at His¹⁵⁹) in the absence of inducing sugar shifts the equilibrium toward the inactive monomer and sequesters LicT by BglP at the cell membrane. In the presence of aryl- β -glucoside (right part of the figure), BglP transfers its phosphoryl group to the incoming sugar, and LicT is no longer phosphorylated on PRD1. Phosphorylation of the PRD2 histidines occurs at high phospho-His-HPr concentration, that is in the absence of glucose, driving LicT toward the firmly closed dimer. Upon dimer closure, the CAT-PRD1 linker helix partially unfolds, allowing CAT to dimerize and interact with RNA. CAT binding to the antiterminator sequence (RAT) in the *bglPH* mRNA prevents formation of the overlapping terminator, and the polymerase can proceed into the downstream coding sequence (bottom right corner).

24, 25), it seems now clear that LicT is phosphorylated on PRD1 and thereby inactivated by its cognate-specific enzyme II (BglP) in the absence of inducing sugar (aryl- β -glucosides). The PRD1 histidines are also substrate for HPr-catalyzed phosphorylation, but the role of these phosphorylation events is less well understood. In the crystal structure of the activated mutant LicT-PRD, both histidines are buried at the PRD1-PRD1' dimer interface and therefore inaccessible to phosphorylating partners. This finding explains why the mutant antiterminator is no more sensitive to BglP-mediated negative regulation (12, 20). Although in the native LicT-PRD structure, the partial opening of the PRD1-PRD1' interface renders His¹⁰⁰ and His¹⁵⁹ accessible to solvent, they still cannot be reached by phosphorylating proteins. Phosphorylation of these histidines would therefore require either an even more open conformation of the PRD1 dimer or dissociation into monomers. According to current models of regulation (8, 26), LicT would become (or stay) monomeric once phosphorylated on PRD1. Based on genetic studies, we have proposed that in the bacterial cells grown in the absence of inducer, BglP sequesters LicT phosphorylated on PRD1 at the cell membrane (13, 20). Upon addition of β -glucoside, BglP would dephosphorylate LicT and release it in the cytoplasm, making it free to interact with RNA (provided it is activated by HPr-catalyzed phosphorylation on PRD2). Recent studies on *E. coli* BglG using fluorescence microscopy show that indeed the antiterminator is recruited at

the bacterial membrane by its cognate enzyme II (BglF) and released upon stimulation (27).

Overall View of the Activation Process—The ensemble of data gathered on LicT now allows proposing a scenario of the activation events, as summarized in Fig. 5. Native LicT is in a dynamic equilibrium between multiple dimer conformers and the monomer (whose folding state remains to be determined). In the monomeric species the histidines in PRD1 would be accessible for (de)phosphorylation, whereas they are not in the native dimer. The monomer may be the major conformational inactive species in the cell, and the present native dimer may be only a species en route to the active dimer. The transition between the inactive and active conformers involves domain motion and conformational switches in the regions linking the three protein modules. The transition between an open inactive and the closed active forms involves conformational switches in the regions linking the three protein modules. Side chain modifications (phosphorylation or substitution) at critical residues drive the equilibrium toward either the inactive conformers or the active closed dimer. Phosphorylation of the PRD1 histidines catalyzed by BglP and/or HPr in the absence of inducing sugar shifts the equilibrium toward the monomer, probably sequestered at the membrane by BglP. Upon exposure of the bacterium to the adequate carbon source (β -glucoside and no glucose or other rapidly metabolizable sugar), phosphorylation by HPr at His²⁰⁷/His²⁶⁹ drives the PRD2 swing and locks both

PRD1 and PRD2 in a closed dimeric conformation. The concomitant remodeling of the linker region between CAT and PRD allows the CAT domain to form a dimer suited for RAT recognition and transcriptional antitermination. This mechanism of activation by domain swing/lock is compatible with a wealth of biochemical and structural data now available for LicT and is likely to apply to other PRD-containing antiterminators.

Acknowledgments—We acknowledge staff from the European Synchrotron Radiation Facility beam lines for help with data collection. We also thank Patrice Vachette and the synchrotron staff at Laboratoire pour l'Utilisation du Rayonnement Electromagnétique for technical assistance in SAXS experiments. We are grateful to Marc Malfois for valuable discussion about the use of OLIGOMER.

REFERENCES

- Hunter, T. (2000) *Cell* **100**, 113–127
- Kruger, S., and Hecker, M. (1995) *J. Bacteriol.* **177**, 5590–5597
- Schnetz, K., Stulke, J., Gertz, S., Kruger, S., Krieg, M., Hecker, M., and Rak, B. (1996) *J. Bacteriol.* **178**, 1971–1979
- Aymerich, S., and Steinmetz, M. (1992) *Proc. Natl. Acad. Sci. U. S. A.* **89**, 10410–10414
- Mahadevan, S., and Wright, A. (1987) *Cell* **50**, 485–494
- Manival, X., Yang, Y., Strub, M. P., Kochoyan, M., Steinmetz, M., and Aymerich, S. (1997) *EMBO J.* **16**, 5019–5029
- van Tilbeurgh, H., Manival, X., Aymerich, S., Lhoste, J. M., Dumas, C., and Kochoyan, M. (1997) *EMBO J.* **16**, 5030–5036
- Declerck, N., Dutartre, H., Receveur, V., Dubois, V., Royer, C., Aymerich, S., and van Tilbeurgh, H. (2001) *J. Mol. Biol.* **314**, 671–681
- Yang, Y., Declerck, N., Manival, X., Aymerich, S., and Kochoyan, M. (2002) *EMBO J.* **21**, 1987–1997
- Postma, P. W., Lengeler, J. W., and Jacobson, G. R. (1993) *Microbiol. Rev.* **57**, 543–594
- Stulke, J., Arnaud, M., Rapoport, G., and Martin-Verstraete, I. (1998) *Mol. Microbiol.* **28**, 865–874
- van Tilbeurgh, H., Le Coq, D., and Declerck, N. (2001) *EMBO J.* **20**, 3789–3799
- van Tilbeurgh, H., and Declerck, N. (2001) *Curr. Opin. Struct. Biol.* **11**, 685–693
- Hendrickson, W. A., and Teeter, M. M. (1981) *Nature* **290**, 107–113
- Lo Conte, L., Chothia, C., and Janin, J. (1999) *J. Mol. Biol.* **285**, 2177–2198
- Svergun, D., Barberato, C., and Koch, M. H. J. (1995) *J. Appl. Crystallogr.* **28**, 768–773
- Konarev, P. V., Volkov, V. V., Sokolova, A. V., Koch, M. H. J., and Svergun, D. I. (2003) *J. Appl. Crystallogr.* **36**, 1277–1282
- Gorke, B. (2003) *J. Biol. Chem.* **278**, 46219–46229
- Fux, L., Nussbaum-Shochat, A., and Amster-Choder, O. (2003) *J. Biol. Chem.* **278**, 50978–50984
- Tortosa, P., Declerck, N., Dutartre, H., Lindner, C., Deutscher, J., and Le Coq, D. (2001) *Mol. Microbiol.* **41**, 1381–1393
- Declerck, N., Vincent, F., Hoh, F., Aymerich, S., and van Tilbeurgh, H. (1999) *J. Mol. Biol.* **294**, 389–402
- Lindner, C., Galinier, A., Hecker, M., and Deutscher, J. (1999) *Mol. Microbiol.* **31**, 995–1006
- Lindner, C., Hecker, M., Le Coq, D., and Deutscher, J. (2002) *J. Bacteriol.* **184**, 4819–4828
- Bachem, S., and Stulke, J. (1998) *J. Bacteriol.* **180**, 5319–5326
- Gorke, B., and Rak, B. (1999) *EMBO J.* **18**, 3370–3379
- Schmalisch, M. H., Bachem, S., and Stulke, J. (2003) *J. Biol. Chem.* **278**, 51108–51115
- Lopian, L., Nussbaum-Shochat, A., O'Day-Kerstein, K., Wright, A., and Amster-Choder, O. (2003) *Proc. Natl. Acad. Sci. U. S. A.* **100**, 7099–7104
- Otwinowski, Z., and Minor, W. (1997) *Methods Enzymol.* **276**, 307–326
- Leslie, A. (1992) *Joint CCP4 and EACMB Newsletter Protein Crystallography*, Daresbury Laboratory, Warrington, United Kingdom
- Brunger, A. T., Adams, P. D., Clore, G. M., DeLano, W. L., Gros, P., Gross-Kunstleve, R. W., Jiang, J. S., Kuszewski, J., Nilges, M., Pannu, N. S., Read, R. J., Rice, L. M., Simonson, T., and Warren, G. L. (1998) *Acta Crystallogr. Sect. D Biol. Crystallogr.* **54**, 905–921
- Terwilliger, T. C. (2002) *Acta Crystallogr. Sect. D Biol. Crystallogr.* **58**, 1937–1940
- Collaborative Computing Project number 4. (1994) *Acta Crystallogr. Sect. D Biol. Crystallogr.* **50**, 760–763